**Bachelorarbeit**
Zur Erlangung des akademischen Grades Bachelor of Science

# Linearisation energies in the LAPW method: Optimizing species files for elemental crystals in exciting.

*Linearsisierungsenergien in der LAPW-Methode: Optimierung von species files für Elementarkristalle in exciting.*

eingereicht von: Lukas Uihlein

Gutachter/innen: Prof. Claudia Draxl
PD Pasquale Pavone

Eingereicht am Institut für Physik der Humboldt-Universität zu Berlin am 23.02.2026

# Contents

## List of Figures



## List of Tables

# 1 Introduction

Thanks to the ever increasing capabilities of modern hardware, numerical methods have become more readily available in material sciences. Kohn-Sham (KS) density-functional theory (DFT) is one of the most widely used numerical methods in solid state physics. It is based on theoretical groundwork from over sixty years ago and provides an *ab-initio* description of a wide range of ground-state properties of bulk crystals, surfaces, molecules, and nanostructures. Over the decades DFT has been continuously refined in many respects. Methodologically most importantly, with regard to the exchange correlation (XC) functionals, which contain the physically significant approximations made by DFT. Regarding the implementation of DFT as a numerical method, many developments were made with regard to the basis sets that are used to expand the KS orbitals in. While plane wave basis sets remain widely used due to their simplicity, their use is computationally expensive. To this end the so-called augmented plane waves (APWs) were developed. However, DFT calculations based on straight APW basis sets are impractical as they would require solving non-linear eigenvalue problems. In view of this, so-called linearized augmented plane wave (LAPW) methods were developed, which, through modifications to the APW basis functions, reduce the task to solving linear equations. The price to be paid for this simplification is referred to as the 'linearization error'. A crucial role in limiting this error, plays the 'linearization energy', a parameter that affects the basis functions. The subject of the present study is to examine three different methods to determine these parameters implemented in the `exciting` code [1].

`exciting` is an all-electron, full potential DFT computer code that implements LAPW methods and supports various different XC functionals. By comparing the different methods to determine linearization energies in `exciting`, this thesis adds to the effort of building a database of flexible, ready-to-use 'species files' meant to facilitate the use of `exciting`.

The thesis is organized as follows: In Section 2, the underlying theory of DFT is explained. Special attention is then given to the APW basis set and the role of trial energies in LAPW methods and their extension in terms of local orbitals (LOs). In Section 3, the specifics of the implementations in `exciting` are presented; first the available methods to determine linearization energies are explained (3.1), then the workflows used to test these methods are illustrated (3.2) and the calculation parameters of the tested systems are reported (3.3). The corresponding computational results are discussed in Section 4 before, finally, drawing some conclusions in Section 5.

# 2 Theoretical Background

## 2.1 Kohn-Sham density functional theory

Density functional theory (DFT) owes its name to its most basic principle: The ground state energy $E_0$ of a system of $N$ interacting electrons in the external Coulomb potential of nuclei $V_{\text{ext}}(\mathbf{r})$ can be expressed as a functional $E[\eta]$ of the spatial electron density $\eta(\mathbf{r})$ rather than as a functional of the full many-electron wavefunction $\psi(\mathbf{r}_1, \mathbf{r}_2, \ldots, \mathbf{r}_N)$ itself [2]. Furthermore, the true electron density $\eta_0(\mathbf{r})$ is the one that minimizes the ground state energy:

$$\begin{aligned}\widetilde{E}[\psi(\mathbf{r}_1, \mathbf{r}_2, \ldots, \mathbf{r}_N)] &= E[\eta(\mathbf{r})] \\ &= T_s[\eta] + E_{\text{ext}}[\eta] + E_{\text{nuc}}[\eta] + E_H[\eta] + E_{\text{XC}}[\eta]\end{aligned} \tag{1}$$

and

$$E[\eta_0(\mathbf{r})] = E_0$$

$T_S$ is the kinetic energy of each electron, $E_{\text{ext}}$ is the energy within the Coulomb potential of the nuclei, $E_{\text{nuc}}$ is the energy from the Coulomb interaction between the nuclei, $E_H$ is the Hartree potential for the electron-electron interaction; $E_{\text{XC}}$ represents the exchange and correlation effects for a given electron density and also corrects for the self-interaction comprised in the Hartree potential.

With regard to finding the ground-state energy of an $N$-electron system this approach reduces the dimensionality of the problem from $3N$ to 3. However, this simplification comes at a price: While not analytically solvable for real-world problems, the form of the Schrödinger equation is known and its solution is exact. In contrast, the explicit form of the energy functional is unknown. Both the kinetic energy $T_{\text{S}}$ and exchange-correlation $E_{\text{XC}}$ parts of the energy functional have no specific form.

Yet, the task to solve this variational problem for the electron density $\eta_0$ was made much more practicable by Kohn and Sham [3]. They showed that the optimal density can be modeled as the of single-electron wavefunctions, the so called Kohn-Sham (KS) orbitals $\psi_i(\vec{r})$:

$$\eta(\mathbf{r}) = \sum_{i}^{\text{occ}} |\psi_i(\mathbf{r})|^2 \tag{2}$$

which are the eigenfunctions to the Kohn-Sham equations:

$$\left[-\frac{\hbar^2}{2m}\nabla^2 + \hat{V}_{\text{ext}} + \hat{V}_{\text{H}}[\eta] + \hat{V}_{\text{XC}}[\eta]\right]\psi_i(\mathbf{r}) = \epsilon_i\psi_i(\mathbf{r}) \tag{3}$$

$\hat{V}_{\text{ext}}$ is the Coulomb potential of the nuclei, $\hat{V}_{\text{H}}[\eta]$ is the Hartree potential of the interacting electrons and $\hat{V}_{\text{XC}}[\eta]$ represents the exchange- and correlation parts of

the potential:

$$\begin{aligned} \hat{V}_{\mathrm{H}}[\eta] &= e^2 \int \frac{\eta(\vec{r}')}{|\vec{r} - \vec{r}'|}\, d^3\vec{r}' \\ \hat{V}_{\mathrm{XC}}[\eta] &= \frac{\delta E_{\mathrm{XC}}[\eta]}{\delta \eta(\vec{r})} \end{aligned} \tag{4}$$

This approach solves the problem of the unknown kinetic energy $T_S$ in Eq.1. The main task that remains is to find an approximation for the exchange-correlation, as it is the only part of Eqs. 3 without a known analytical form.

The most basic of these approximations is the local density approach (LDA), where the exchange-correlation energy term is estimated locally based on the energy of the uniform electron gas of that same density. Slightly more complex is the general gradient approximation (GGA), which uses both the electron density and its gradient to locally approximate the exchange correlation energy term. Over the years various more elaborate approximations have been developed, tested and implemented. However, no 'one size fits all' approximation has emerged as a best way to treat most or even all systems [4, 5].

Another complication is that the electron density function appears in the $\hat{V}_{\mathrm{H}}$ and $\hat{V}_{\mathrm{XC}}$ terms of the KS equations, constituting a self-referential problem: In order to determine $\eta(\vec{r})$ as a sum of the KS orbitals as per Eq. 2, we need need $\eta(\vec{r})$ to construct and solve the KS equations 3. The way out of this circularity is to use an iterative procedure: Make an initial educated guess for $\eta(\mathbf{r})$ and then alternately solve the KSEs and calculate a new electron density based on these KS orbitals. Convergence can be established with regard to the electron density and the total ground-state energy, for which the variational principle holds.[1] Hence, ideally the calculated total ground-state energy decreases steadily across iterations until the energy difference between two subsequent iterations falls below a specified threshold.

In this self-consistent field (SCF) loop, the main task is to solve the KS equations. This can be done either on a spatial grid or by expanding the KS orbitals in some basis $\Phi_j \in L^2(\mathbb{R}^3)$ and finding approximate solutions with regard to this basis. In the latter case, the task boils down to the diagonalization of matrices and we can express the KS equations in terms of an eigenvalue problem:

$$(\hat{\mathbf{H}} - \epsilon_\nu\, \hat{\mathbf{S}}) \cdot \mathbf{c}_\nu = 0 \tag{5}$$

where $\mathbf{c}_\nu$ represent the eigenfunctions, $\hat{\mathbf{H}}$ the Hamiltonian and $\hat{\mathbf{S}}$ the overlap matrices

[1] Convergence of total energy is a necessary but not sufficient criterion for establishing convergence. In actual implementations, there are additional convergence criteria for other parameters, e.g., electron density.

with regard to the basis functions $\Phi_j(\mathbf{r})$:

$$\begin{aligned}\psi_\nu(\mathbf{r}) &= \sum_j c_{\nu j}\Phi_j(\mathbf{r}) \\ \mathrm{H}_{ij} &= \langle\Phi_i| -\frac{\hbar^2}{2m}\nabla^2 + \hat{V} + \hat{V}_\mathrm{H} + \hat{V}_\mathrm{XC}|\Phi_j\rangle \\ S_{ij} &= \langle\Phi_i|\Phi_j\rangle\end{aligned}$$

Finding the eigenvectors $\mathbf{c}_\nu$, i.e. solving the secular equation 5, makes up the majority of the computational cost of each iteration in the SCF loop. Therefore it is of great value to optimize this process. One of the most important factors in this regard is the choice of basis functions $\Phi_j$. A lot of effort has been put into the development of different basis sets that allow for a sufficiently accurate representation of the KS orbitals, while at the same time not requiring an unnecessary large amount of basis functions. The last part is important because the size of $\hat{\mathbf{H}}$ and $\hat{\mathbf{S}}$ both scale as the cube of the number of basis functions. Furthermore, basis sets should ideally be of some generic form, so that they can easily be adapted for use with a range of different systems or materials.

For spatially periodic systems like crystals, the use of plane waves seems an obvious choice in this regard, as for their ease of use and theoretical completeness. However, plane waves are inefficient at representing KS orbitals, because the KS orbitals are very fast varying in vicinity of nuclei, but only change comparatively slowly more far out. Accordingly, a very wide range of plane wave frequencies or rather a high energy cutoff has to be used in order to represent both properties accurately, which leads to large dimensions in the secular equation.

Generally, there are two approaches to solving this problem: the first is to get rid off the fast-varying behavior of the wave-functions altogether; the other is to handle the fast-varying behavior by the use of basis functions that are themselves fast-varying in the respective areas. In the former approach the singularity in the Coulomb potential is removed by modeling a so-called pseudopotential: a smooth potential describing the charge distribution from both the nuclei and the closely bound core electrons. Removing the singularity from the potential also removes any fast varying behavior from the wave functions of the remaining valence electrons. These solutions can then be accurately described by a plane waves basis with a relatively low cut-off energy. However, this approach comes with some caveats: the construction of suitable pseudopotentials is cumbersome and, more importantly, it introduces an approximation that violates the validity of the variational principle. For a more detailed account see e.g. [5, 24ff.].

The second approach tries to avoid further approximations, but uses more elaborate basis functions in order to reduce the necessary size of the basis. One implementation of this idea is the so-called augmented plane wave method, which is discussed in the following subsection.

## 2.2 The augmented plane wave method

The basic idea of the augmented plane wave (APW) methods is for the basis functions directly to mimic the behavior of the KS orbitals. To this purpose, space is partitioned into so-called Muffin-tin (MT) spheres $S_\alpha$ with radius $R_{\mathrm{MT}}$ around the nuclei $\alpha$. The space in between the MT spheres is called the interstitial region $I$.The desired basis functions $\Phi_j(\mathbf{r})$ are fast varying in the MT spheres, but are plane waves beyond the threshold distance of $R_{\mathrm{MT}}$, i.e. in the interstitial region.

Evidently, the choice of basis functions inside the MT spheres is the pivotal point in this approach. In the original paper Slater [6] proposed the use of solutions to the simplified problem, where the potential is spherically symmetrical inside the MT spheres and constant in the interstitial region.[2] With the Bloch boundary conditions for periodic potentials the solutions to this simplified problem with regard to a given MT sphere $S_\alpha$ can be written as:

$$\Phi^{\mathbf{k}+\mathbf{G}}(\mathbf{r}) = \begin{cases} \Omega^{-1/2} e^{i(\mathbf{k}+\mathbf{G})\mathbf{r}}, & \mathbf{r} \in I \\ \sum_{\ell m} A^{\mathbf{k}+\mathbf{G}}_{\alpha\ell m} u_{\alpha\ell}(r_\alpha) Y_{\ell m}(\hat{\mathbf{r}}_\alpha), & \mathbf{r} \in S_\alpha \end{cases} \tag{6}$$

Here $\mathbf{G}$ are the reciprocal lattice vectors, $\mathbf{k}$ is the basis elements' wave vector within the first Brillouin zone and $\Omega$ is the volume of the unit cell. $\ell$ and $m$ are the angular momentum and magnetic quantum numbers respectively of the corresponding spherical harmonics $Y_{\ell m}(\hat{\mathbf{r}}_\alpha)$ and the radial functions $u_{\alpha\ell}(r_\alpha)$. $r_\alpha = |\mathbf{r} - \mathbf{R}_\alpha|$ is the radial distance to the nucleus at the center $\mathbf{R}_\alpha$ of the respective MT sphere $\alpha$, while $\hat{\mathbf{r}}_\alpha = \frac{\mathbf{r}-\mathbf{R}_\alpha}{r_\alpha}$ is the corresponding angular component. The coefficients $A^{\mathbf{k}+\mathbf{G}}_{\alpha\ell m}$ are fixed by the requirement for $\Phi^{\mathbf{k}+\mathbf{G}}_\alpha(\mathbf{r})$ to be continuous along the MT sphere. The functions $u_{\alpha\ell}$ are the solutions to the radial part of the Schrödinger equation:

$$\left[ -\frac{\mathrm{d}^2}{\mathrm{d}^2 r_\alpha} + \frac{\ell(\ell+1)}{r_\alpha^2} + v_{\alpha 0}(r_\alpha) - \epsilon \right] r_\alpha \; u_{\alpha\ell}(r_\alpha) = 0 \tag{7}$$

$v_{\alpha 0}(r_\alpha)$ includes the Coulomb potential from the nucleus at the center of the respective MT sphere $\alpha$ and the average Coulomb potential from the other nuclei in the unit cell, and $\epsilon$ is the energy of the respective solution.

This APW basis is much more efficient at accurately depicting the KS orbitals than a simple plane wave basis is, i.e. the necessary cutoff-frequency is much lower. However, there is a considerable drawback to actually using this APW basis set in the SCF method of DFT: As per Eq. 7, the radial functions $u_\ell$ depend on the energy of the respective state, hence the APW basis set as a whole depends on the set of eigenenergies $\{\, \epsilon_i \,\}$ of the KSEs. Accordingly, the secular equation 5 becomes

[2] Originally Slater made the simplification of zero potential in the interstitial region. However, the generalization to an arbitrary, constant non-zero potential is straightforward and corresponds to factoring in the average Coulomb potential from the other nuclei outside the respective MT sphere $S_\alpha$ in $v_{\alpha 0}(r)$ in Eq. 7.

a non-linear equation, making it much more costly to solve:

$$(\hat{\mathbf{H}}(\{\,\epsilon_i\,\}) - \epsilon_i \hat{\mathbf{S}}(\{\,\epsilon_i\,\}) \cdot \mathbf{c}_i = 0$$

In each iteration of the SCF loop, the secular equation itself has to be solved self-consistently with regard to the set of $\epsilon_i$. To further complicate matters, the eigenfunctions and -energies depend on the respective wave vector, hence the secular equation has to be solved at every **k**-point individually, making non-linear equations even more undesirable.

One way to circumvent a non-linear secular equation is to set fixed energy parameters $E_\ell$ – hereinafter referred to as linearization energies – when building the $u_\ell$ via Eq. 7. This is referred to as linearized augmented plane wave (LAPW) method.

### 2.2.1 The linearized augmented plane wave method

The central issue with using linearization energies $E_\ell$ instead of the actual eigenenergies $\epsilon_i$ in Eq.7, is that the solutions $u_\ell$ are very sensitive to this parameter and the resulting basis set may no longer be adequate to represent the respective KS orbitals. The resulting errors are commonly termed, 'linearization errors'. The key task of LAPW methods is to use fixed linearization energies to achieve linearization of the problem, while keeping these errors as small as possible. For this, the APW basis set is altered and/or extended.

The most common LAPW variant uses a Taylor-like expansion of the radial functions $u_\ell$ from the regular APWs with respect to the linearization energies $E_\ell$:

$$u_\ell(r, \epsilon) = u(r, E_\ell) + (\epsilon - E_\ell)\ \dot{u}(r, E_\ell) + \mathcal{O}((\epsilon_i - E_\ell)^2) \tag{8}$$

$\dot{u}_\ell$ is the derivative of $u_\ell(r;\epsilon)$ with regard to $\epsilon$, satisfying the equation:

$$\left[-\frac{\mathrm{d}}{\mathrm{d}r^2} + \frac{\ell(\ell+1)}{r^2} + v_0(r) - E_\ell\right] r\ \dot{u}_\ell(r, E_\ell) = r\ u_\ell(r, E_\ell) \tag{9}$$

The basis set obtained from this expansion may be written as

$$\Phi^{\mathbf{k}+\mathbf{G}}(\mathbf{r}) = \begin{cases} \Omega^{-1/2} e^{i(\mathbf{k}+\mathbf{G})\mathbf{r}}, & \mathbf{r} \in I \\ \sum_{\ell m} \left[A^{\mathbf{k}+\mathbf{G}}_{\alpha\ell m} u_{\alpha\ell}(r_\alpha, E_\ell) + B^{\mathbf{k}+\mathbf{G}}_{\alpha\ell m} \dot{u}_{\alpha\ell}(r_\alpha, E_\ell)\right] Y_{\ell m}(\hat{\mathbf{r}}_\alpha), & \mathbf{r} \in S_\alpha \end{cases} \tag{10}$$

The coefficients $A^{\mathbf{k}+\mathbf{G}}_{\alpha\ell m}$ and $B^{\mathbf{k}+\mathbf{G}}_{\alpha\ell m}$ are set to achieve continuity of $\Phi^{\mathbf{k}+\mathbf{G}}_\alpha(\mathbf{r})$ at the boundary of MT sphere $S_\alpha$, both in value and slope. This basis set proves way more flexible with regard to the linearization energies, i.e. linear combinations of $u_{\alpha\ell}(r_\alpha, E_\ell)$ and $\dot{u}_{\alpha\ell}(r_\alpha, E_\ell)$ are better suited to replicate the desired radial function $u_{\alpha\ell}(r_\alpha, \epsilon)$ than just the $u_{\alpha\ell}(r_\alpha, E_\ell)$ alone.

The expansion of the radial wave function 8 allows for an estimation of the

linearization error arising from using a fixed set of $E_\ell$ instead of $\epsilon_i$ when creating the basis set. The error in the wave functions and band energies is of order $(\epsilon - E_\ell)^2$, the resulting error in calculated total energies are of order $(\epsilon - E_\ell)^4$[7, 8].[3]

In principle, this expansion can be extended to include higher order derivatives $u_\ell$, reducing the linearization error, as in the so-called quadratic (QLAPW) or super LAPW (SLAPW) methods [9]. However the resulting basis functions become increasingly stiff, i.e. plane wave like, towards the MT sphere boundary, making them less suited to replicate the distinctive fast varying behavior inside the MT spheres. To compensate for this, a higher plane-wave cutoff is necessary, which comes at the expense of an increase in basis size and the corresponding computational effort [5]. A more efficient and generally more flexible way to further reduce the linearization error is the the 'local-orbital' extension, which is explained in some more detail in the following.

### 2.2.2 Local orbitals

The APW basis functions aim to describe electronic states that are, at least to some degree, delocalized. Yet in most crystals only the valence states require such a description, while most occupied states do not show any significant dispersion, but are strongly localized at a specific atom. Accordingly, these states are usually denoted as 'core-states' and can be accounted for separately by solving the the single-electron atomic problem to obtain the respective KS orbitals.

However, not all non-valence states, can be taken care of that easily. There may occur, so called 'semi-core' states, for which interactions with other atoms are not as easily neglectable because they are spaciously more extended than the core-states. One option to deal with these states is to treat them just like the valence states, i.e. in terms of the APW basis functions. However, this can only be achieved with considerable additional effort: since the respective basis functions in each $\ell$-channel cannot describe both the valence and semi-core state simultaneously, two separate calculations must be performed, where the linearization energy of the APW basis function is selected once for the valence and semi-core state respectively. This is referred to as the multiple-window approach [5, 83ff].

A generally more efficient way of dealing with semi-core states is to extend the basis set with so-called 'local-orbital' functions (LOs) $\phi_\mu^{LO}(\mathbf{r})$. Inside the MT spheres, these functions are of equal form as the APW basis functions, but instead of transitioning into a plane wave, they disappear at the edge of the muffin tin sphere:

$$\phi_\mu^{LO}(\mathbf{r}) = \begin{cases} 0, \ \mathbf{r} \in I \\ \left[a_\mu u_{\alpha\ell}^{(i)}(r_\alpha, E_\ell^{LO}) + b_\mu u_{\alpha\ell}^{(j)}(r_\alpha, E_\ell^{LO})\right] Y_{\ell m}(\hat{\mathbf{r}}_\alpha), \ \mathbf{r} \in S_\alpha \end{cases} \tag{11}$$

[3] The error estimates are in relation to the 'true' eigenenergy derived from solving the non-linear problem self-consistently as one would, when just using the APW basis set.

$\mu$ is an arbitrary numbering index, $(i)$ and $(j)$ indicates the order of the derivative of the radial function. The coefficients $a_\mu$ and $b_\mu$ by the requirement of a smooth transition to zero at $R_{\mathrm{MT}}$. The exact form of the LOs used in DFT-implementations may vary, most notable, there are differences (1) with regard to the orders of the energy derivatives of the radial functions $u_\ell$ they include and (2) whether they use an linearization energy $E_\ell^{LO}$ that is different from the energy parameter $E_\ell$, that is for constructing the complementary APWs (see e.g. [1, 10, 11]).

Besides dealing with semi-core states, the LO extension improves greatly the basis' overall flexibility within the MT spheres, which is why they are suited to reduce the linearization error. To this end the expansion with regard to the energy parameter has proven to be more efficient for LOs than for the APWs (Eq. 10 or the QLAPW and SLAPW approaches). Accordingly, they are commonly used as an extension to basis sets as defined in Eq. 6, which is then referred to as APW+lo basis sets. But they may also be used with basis sets of type 10, then often referred to as LAPW+lo basis sets. LOs also prove useful for various other purposes, e.g. to describe high-angular momentum and high-energy components in calculations of excited states[12].

# 3 Implementation and methodology

## 3.1 Determination of linearization energies

As explained in Section 2, the linearization energies $E_\ell$ play an important role in the LAPW methods as they substantially affect the size of the linearization error. However, little has been said on how to actually determine useful values for $E_\ell$ without generating too much computational overhead. The literature mentions a few different approaches to this problem, three of which are implemented in `exciting`.

### 3.1.1 Wigner-Seitz method

The most straightforward way of determining linearization energies in `exciting` is based on the so-called 'Wigner-Seitz rules'. Andersen [13] refers to them as a way to estimate the maximal and minimal energies, $\epsilon_\ell^{\max}$ and $\epsilon_\ell^{\min}$, within a given energy band $\nu$ of predominantly $\ell$-character. The idea is then to simply set the linearization energy at the center of this energy window:

$$E_{\nu\ell}^{\mathrm{ws}} = \frac{\epsilon_{\nu\ell}^{\max} - \epsilon_{\nu\ell}^{\min}}{2} \tag{12}$$

$\epsilon_\ell^{\min}$ and $\epsilon_\ell^{\max}$ are derived as the roots of the radial function and its spacial derivative at the Muffin-tin sphere, respectively:

$$\left.\frac{\partial\, u_\ell(r, \epsilon_{\nu\ell}^{\max})}{\partial\, r}\right|_{r=R_{\mathrm{MT}}} = 0$$

and

$$\left. u_\ell(r, \epsilon_{\nu\ell}^{\min})\right|_{r=R_{\mathrm{MT}}} = 0$$

The solutions to the above equations can be ascribed to a different energy band by counting the number of knots of the respective $u_\ell$ within the MT sphere. Choosing a linearization energy within the $[\epsilon_{\nu\ell}^{\min}, \epsilon_{\nu\ell}^{\max}]$ window then ensures to keep the adequate number of $\nu - \ell - 1$ knots within the muffin sphere and corresponds to ideal binding ($\epsilon_\ell^{\max}$) or anti-binding ($\epsilon_\ell^{\min}$) character for the given $\ell$-channel [14]. In `exciting` the algorithm searching for these Wigner-Seitz linearization energies uses a hard-coded fallback value of 1.0 $E_{\mathrm{h}}$ if it fails to find the proper energy window. In practice this happens mostly for high $\ell$-channels. Despite their simplicity, the Wigner-Seitz rules have proven reliable in implementations; not only in `exciting`, but also in the WIEN2k DFT package [15, 16] for example.

### 3.1.2 '$\ell$-like' charge method

The method referred to as '$\ell$-like' charge or 'lcharge' method was introduced by Blügel and Bihlmayer [17]. It takes a much more sophisticated approach to deter-

mining linearization energies, taking into account (1) multiple energy bands and (2) the **k**-dependency of the energy within a band.
To achieve (1), the density of '$\ell$-like' charge in a band $\nu$ is derived from the corresponding eigenfunctions $\psi_{\nu\ell}$ at each **k**-point:

$$n_{\nu\ell}(\mathbf{k}) = \int_{\mathrm{MT}} |\psi_{\nu\ell}(\mathbf{r},\mathbf{k})|^2 \,\mathrm{d}^3 r \tag{13}$$

To account for (2), the quadratic difference between the bandenergy and linearisation parameter is calculated at each **k**-point and summed up for all occupied states, that is states where the bandenergy $\epsilon_\nu(\mathbf{k})$ is below the Fermi-energy $E_\mathrm{F}$:

$$\int_{\mathrm{BZ}} \sum_{\nu}^{\epsilon_\nu(\mathbf{k})<E_\mathrm{F}} \left(\epsilon_\nu(\mathbf{k}) - E_\ell\right)^2 \mathrm{d}^3 k \tag{14}$$

This difference is then weighted according to 13, i.e. by how much a specific **k**-point in given band $n$ contributes to the total charge of each $\ell$-type, in order to derive a criterion for the quality of the linearization energies:

$$\Delta E_\ell = \int_{\mathrm{BZ}} \sum_{\nu}^{\epsilon_\nu(\mathbf{k})<E_\mathrm{F}} \left(\epsilon_\nu(\mathbf{k}) - E_\ell\right)^2 n_{\nu\ell}(\mathbf{k}) \mathrm{d}^3 k \tag{15}$$

In the lcharge-method, the linearization energies $E_\ell^{\mathrm{lc}}$ are set to minimize the $\Delta E_\ell$.

Compared to the implementation of the Wigner-Seitz rules this method comes with some drawbacks. Most apparently there is the computational effort to calculate the $\ell$-resolved density of states. More fundamentally though, this method relies on the explicit knowledge of the eigenfunctions and -energies, i.e. on the solutions to the problem we are trying to solve, invoking the same problem that induced the development of LAPW methods in the first place. However, within the SCF loop this problem can be circumvented by utilizing the eigenfunctions and -energies from the previous iteration. For the first iteration the basis functions are generated at a specified default energy, which in this study was set to 0.15 $E_\mathrm{h}$ for all basis functions in all calculations.

Most importantly though, unlike the Wigner-Seitz rules, the lcharge method can not distinguish between different energy bands, as it averages across different bands. Accordingly, minimizing Eq. 15 yields only one linearization energy $E_\ell^{\mathrm{lc}}$ for each $\ell$-channel, which makes it impossible to treat semi-core and valence states separately.

### 3.1.3 Logarithmic derivative method

The third method to set the linearization energies relies on the logarithmic derivative of the radial functions at the MT sphere boundary:

$$D_\ell(\epsilon) = \frac{\mathrm{d}}{\mathrm{d}r}\log(u_\ell(r,\epsilon))\bigg|_{r=R_{\mathrm{MT}}} = \frac{u'_\ell(r,\epsilon)}{u_\ell(r,\epsilon)}\bigg|_{r=R_{\mathrm{MT}}} \tag{16}$$

The linearization energies $E^{\mathrm{ld}}_{\nu\ell}$ are chosen so that

$$D_\ell(E^{\mathrm{ld}}_{\nu\ell}) = \frac{-(\ell+1)}{R_{\mathrm{MT}}} \tag{17}$$

is satisfied, which correspond to the evanescent solutions of Eq. 7 with $v_{\alpha 0}(r_\alpha) = 0$[7, 10]. The behavior of $D_\ell(E)$ is similar to the cotangent, diverging at energies, where a knot of $u_\ell$ 'passes through' the MT sphere boundary. Accordingly Eq. 17 yields a solution for each branch of the graph, attributable to an energy band in the respective $\ell$-channel via the number of $\nu - \ell - 1$ knots inside the MT sphere. The method is based on the work of Andersen [8] estimating the accuracy of the LAPW method against the KKR and LMTO methods, and is referred to in early applications of the LAPW method [7]. More recently, the method was used to construct local orbitals descriptive of high energy [10] and semi-core states[11].

### 3.1.4 'no-search' method

The simplest method in `exciting` is referred to as the 'no-search' method. While the implementation of the before mentioned methods update the linearization energies in every[4] iteration of the SCF cycle, this method sets them only in the first iteration and then keeps them constant over the course of the entire `exciting` calculation. Hence, also the same basis functions are used for the entire SCF loop. In the first iteration the linearization energies are set following the Wigner-Seitz procedure, however, only for those $\ell$-channels that have at least one occupied non-core state specified. For all other basis functions the linearization energy is set to a default value. In principle, this value could be adjusted for each function individually, however in this study it was kept at 0.15 $E_{\mathrm{h}}$ for all calculations and basis functions.

## 3.2 Methodology

In order to test these different methods, each of them is deployed in two workflows from the `exciting` workflow package. The package builds on the `excitingtools` package [18] to facilitate high throughput `exciting` calculations. Among other things, it implements an easy and consistent way to build basis sets, that can be

[4] To be more precise, the lcharge method skips the calculation new linearization energies if the change of effective potential between the respective SCF iterations falls below a specified threshold.

summarized as a two-step process: (1) build a basis set as large as possible (without running into computational issues) in order assess the maximum attainable accuracy and (2) systematically reduce the basis size, tracking the change in total energy per atom in order to assess the minimum required basis size for a given target accuracy. Before explaining the methodology underlying these workflows in more detail however, it is first necessary to explain the used basis sets in more detail.

### 3.2.1 Basis sets

As already indicated, the concepts explained in the Section 2 allow for some mixing and matching, resulting in a variety of different basis sets. `exciting` captures this diversity, and allows to define the included basis functions for each state in each atomic species individually. The specific basis sets used in the workflows consist of APWs and two different types of LOs.

The APWs are generated according to Eq. 10, featuring the first order energy derivative of the radial function as defined in Eq. 9. For each valence state the basis set includes one such APW basis function. For $\ell$-channels with only core-states, an APW is added the the lowest lying unoccupied state up to $\ell = 12$. The linearization energies are determined via the index $\nu$ and $\ell$-character of the respective band. The first type of LOs can be defined via:

$$\phi_{\nu\ell m}^{\alpha(i,i+1)}(\mathbf{r}) = \begin{cases} 0, \ \mathbf{r} \in I \\ \left[a_{\nu\ell m}^{\alpha} u_{\alpha\ell}^{(i)}(r_\alpha, E_{\nu\ell}^{\alpha}) + b_{\nu\ell m}^{\alpha} u_{\alpha\ell}^{(i+1)}(r_\alpha, E_{\nu\ell}^{\alpha})\right] Y_{\ell m}(\hat{\mathbf{r}}_\alpha), \ \mathbf{r} \in S_\alpha \end{cases} \tag{18}$$

Here $u_{\alpha\ell}^{(i)}(r, E_{\nu\ell})$ is the $i$-th energy derivative of $u_\ell$, $Y_{\ell m}(\hat{\mathbf{r}})$ are the spherical harmonics and the coefficients $a_{\alpha\ell m}$ and $b_{\alpha\ell m}$ are set so that the function approaches zero continuously at the edge of the sphere. Notably, these LOs only feature a single linearization energy $E_{\nu\ell}$, determined according to the respective $\nu$ and $\ell$ of the valence or semicore state. [For the valence states these LOs are therefore very similar to parts of the respective APWs. The advantage of adding LOs then results from the combination of $u_\ell$ derivatives of different (higher) orders and the coefficients that are adjusted to satisfy different boundary conditions than for the APWs.] In `exciting` workflows, the comprised orders of energy derivatives $(i, i+1)$ are sometimes referred to as 'matching orders'. The initial basis set features LOs $\phi_{\nu\ell m}^{\alpha(i,i+1)}$ of matching orders $(0, 1)$, $(1, 2)$ and $(2, 3)$ and all possible values of $m$ for each non-core state.

The second type of LO is added only for semicore states and may be written as:

$$\varphi_{\ell m}^{\alpha}(\mathbf{r}) = \begin{cases} 0, \ \mathbf{r} \in I \\ \left[c_{\ell m}^{\alpha} u_{\alpha\ell}^{(0)}(r_\alpha, E_{\nu\ell}^{\alpha}) + d_{\ell m}^{\alpha} u_{\alpha\ell}^{(0)}(r_\alpha, E_{(\nu-1)\ell}^{\alpha})\right] Y_{\ell m}(\hat{\mathbf{r}}_\alpha), \ \mathbf{r} \in S_\alpha \end{cases} \tag{19}$$

As above, the coefficients $c_{\ell m}^{\alpha}$, $d_{\ell m}^{\alpha}$ are set to ensure a smooth transition to zero at

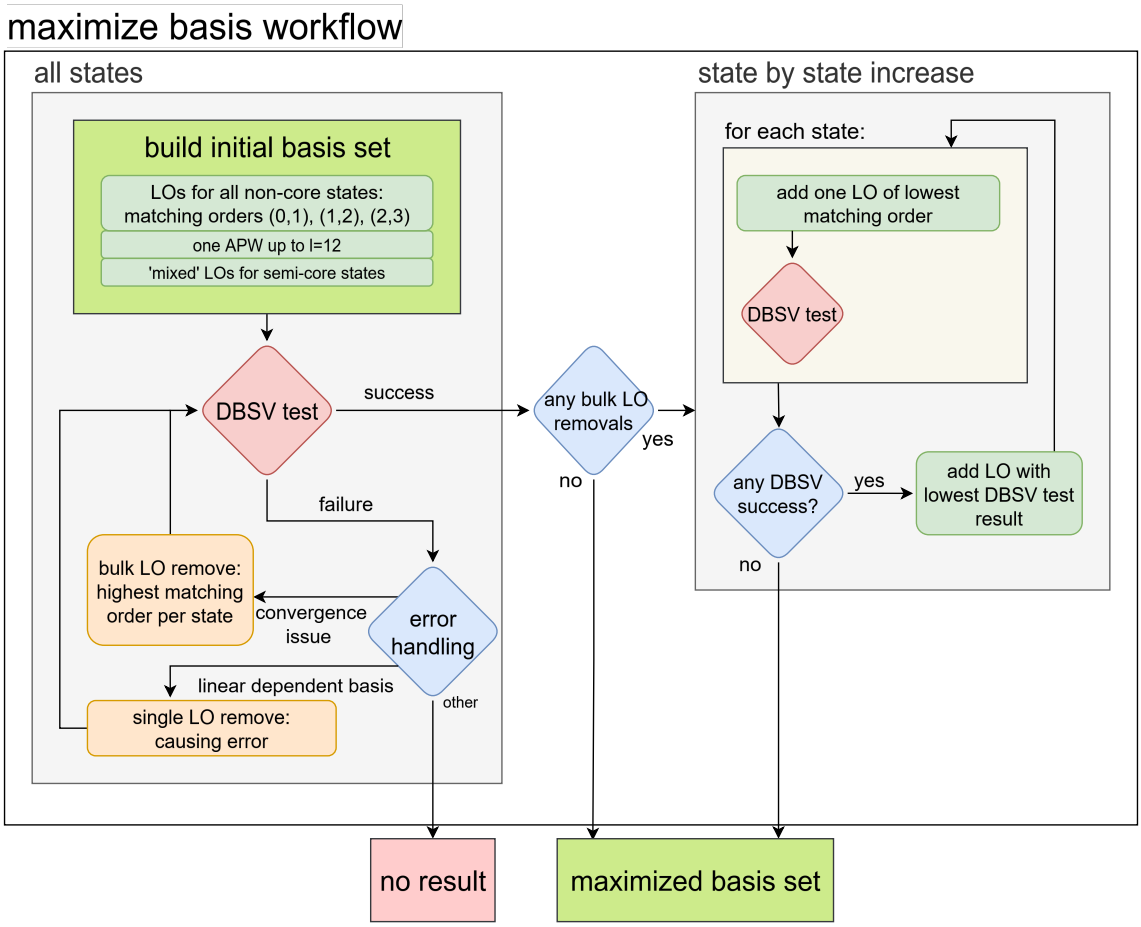


Figure (1) Flowchart of the 'maximize basis' workflow

$R_{\mathrm{MT}}$. These LOs do not feature any energy derivatives of $u_\ell$, but combine radial functions generated at the linearization energies of the valence band $E_{\nu\ell}$ and semicore states $E_{(\nu-1)\ell}$ in the respective $\ell$-channel. For each semicore state, the basis includes these 'mixed' LOs $\varphi^{\alpha}_{\ell m}$ for all possible $m$-values.

A more detailed outline of the specific computational implementations of generating basis functions in `exciting` can be found in [1].

### 3.2.2 `exciting` workflows

Flowcharts of the workflows are depicted in Figs. 1 and 2. The maximize species workflow starts out with an initial basis set as explained above. If the calculation fails, LOs are removed successively: in case linear dependencies in the basis set, the LO [most likely] causing the issues is removed specifically; in case of convergence problems, the LOs with the highest energy derivative combination are removed for each state. In the latter case, the workflow later tries to add them back to the basis one-by-one, if the removal across all states lead to a successful calculation. If successful, the maximize basis workflow outputs a basis set that is then be put into the LO hierarchy workflow.

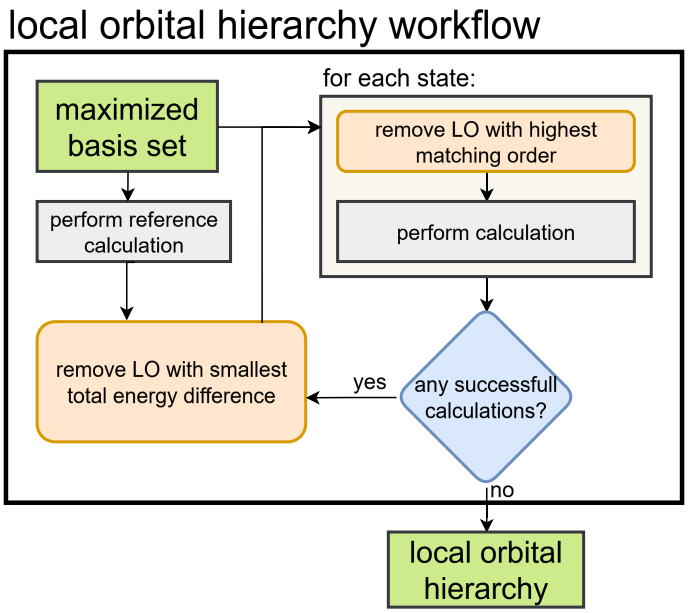


Figure (2) Flowchart of the LO hierarchy workflow

The LO hierarchy records the difference in total energy per atom, when *provisionally* removing the LO of highest matching order for each state *individually*. The LO with the lowest energy difference is then *permanently* removed from the basis set, which is then used to repeat this process. The resulting output allows to define a hierarchy of the LOs, i.e. a record of how much of the total energy per atom can be ascribed to a specific LO.

The 'dual-basis self-validation' (DBSV) test [12] is used to assess the quality of the basis set. It evaluates the total ground state energy per atom of a test calculation against a benchmark calculation. For this benchmark calculation, the MT radius is decreased from `autormt` = 0.95 to `autormt` = 0.75 of the maximum possible value (where adjacent MT spheres would begin to intersect) and the plane wave cutoff is notably increased. The idea is that for small MT radii, more space is covered by the interstitial plane wave basis; and the description via plane waves allows for a systematic increase in accuracy at the cost of higher computational effort by simply increasing the plane wave cutoff. Hence, the smaller the energy-difference between small and large MT radius calculations, i.e. the DBSV result $\Delta E_{\mathrm{DBSV}}$, the better is the respective basis set. The DBSV test therefore indicates how well a linear combination of LOs and APWs represents the KS orbitals in the outer shell of the MT spheres; compared to the systematic expansion of that part of the KS orbital in plane waves.[5]

The results from the maximize basis workflow allow for a comparison of the maximal attainable accuracy of the ground state total energy, when using the different

[5]To this end the basis itself has to remain unchanged in the benchmark calculation. The linearization energies are therefore copied from the test calculation, as a change in MT radius would otherwise also affect the resulting basis functions.

methods to set the linearization energies. Results from the LO hierarchy workflows allow for comparing the 'efficiency' of the individual LOs generated with these methods. It is important to note that the results only refer to the specific 'construction plan' for the basis set as defined in the workflows.[6] However, this specific choice of basis set assembly and disassembly was made by the authors with some consideration; and in view of limiting this study's computing time, keeping this 'variable' constant allowed for the examination of a comprehensive set of different elemental crystals.

### 3.3 Test systems and calculation parameters

The workflows were run for each of the four methods discussed in 3.1. As test systems served same elemental crystals that were also used in the comprehensive Delta DFT study [19]. For 69 out of these 71 structures, input files were readily available, that are well-converged with regard to the density of the **k**-point grid and and relaxed with regard to the lattice parameters. However, the calculations performed for the present study did not take into account the relativity of the valence states, as the DBSV test method is not compatible with the jumps in total energy that occur when the MT radius changes. Apart from that all parameters not directly implicating the basis or MT radius were transferred. A comprehensive layout of all these parameters can be found in the Delta DFT study's supplementary material.[7]

[6] For example, one could change the types of LOs to be added, change the test order of the individual LOs in the LO hierarchy workflow or vary the number of unoccupied states taken into account.

[7] The entire calculation data will be uploaded to the NOMAD database [20] some time in the future. As for now, the bulk uploading of large chunks of data is unstable.

| | | **'no-search'** | **Wigner-Seitz** | **log. derivative** | **lcharge** |
|---|---|---|---|---|---|
| # | successfull runs | 67 | 67 | 34 | 1 |
| # | best $\Delta E^{\max}_{\mathrm{DBSV}}$ results | 54 | 7 | 7 | 0 |
| | mean log $\frac{\Delta E^{\max}_{\mathrm{DBSV}}}{E_{\mathrm{h}}}$ | 5.3e-5 | 4.2e-4 | 2.4e-2 | (9.5e-2) |
| # | $\Delta E^{\max}_{\mathrm{DBSV}} < 10^{-2}\ E_{\mathrm{h}}$ | 59 | 58 | 14 | 0 |
| # | $\Delta E^{\max}_{\mathrm{DBSV}} < 10^{-4}\ E_{\mathrm{h}}$ | 46 | 20 | 5 | 0 |
| # | $\Delta E^{\max}_{\mathrm{DBSV}} < 10^{-6}\ E_{\mathrm{h}}$ | 8 | 7 | 5 | 0 |
| | avg. SCF iterations | 13 | 13 | 22 | (16) |
| | avg. basis size/atom | 38 | 38 | 26 | (24) |

Table (1) Summary of the results from the 'maximize basis' workflow runs

# 4 Computational results

## 4.1 Maximized basis sets

Table 1 gives an overview of the results from the maximal possible basis, as output by the 'maximize basis' workflow. In Figure 3, a boxplot displays the $\Delta E^{\max}_{\mathrm{DBSV}}$ results of the these basis sets derived from the workflows for the 'no-search', Wigner-Seitz and logarithmic derivative methods. The '$\ell$-like charge method' is not included, because the 'maximize basis' workflow runs failed for all but one element. Most runs failed due to degenerate radial functions in the LOs or APW functions (62 out of 69). In as many as 40 cases the calculation failed during the first SCF iteration, when the linearization energies are uniformly set to the starting value of 0.15 $E_{\mathrm{h}}$. Accordingly, an adjustment of these starting energy values or an implementation of the Wigner-Seitz method for the first iteration might salvage the workflow for some elements. However as explained earlier, the main issue seems to be that this method does not distinguish between different bands within an $\ell$-channel, which renders the inclusion of the LOs ineffective at dealing with semicore states. The '$\ell$-like charge method' method is therefore not taken into account in the further evaluation.

Regarding the other three methods, for 54 out of 69 elements elements keeping the linearization energies constant resulted in the most precise maximized basis set in terms of $\Delta E^{\max}_{\mathrm{DBSV}}$. Reaching $\Delta E^{\max}_{\mathrm{DBSV}} < 10^{-4}\ E_{\mathrm{h}}$ and $< 10^{-6}\ E_{\mathrm{h}}$ in 46 and 8 cases respectively. The Wigner-Seitz method yields similar, but overall less consistent basis sets, with 20 elements below $10^{-4}\ E_{\mathrm{h}}$ precision and 7 at $10^{-6}\ E_{\mathrm{h}}$ in terms of $\Delta E^{\max}_{\mathrm{DBSV}}$. The logarithmic derivative method is mostly unreliable workflow, often exceeding the limit of 40 SCF iterations without reaching convergence (30 cases) or failing in the diagonalization of the Hamiltonian matrix (five cases). Yet, for seven elements this method yielded the lowest value for $\Delta E^{\max}_{\mathrm{DBSV}}$.

Figure 4 shows the results of the 'maximize basis' workflow runs in more detail.

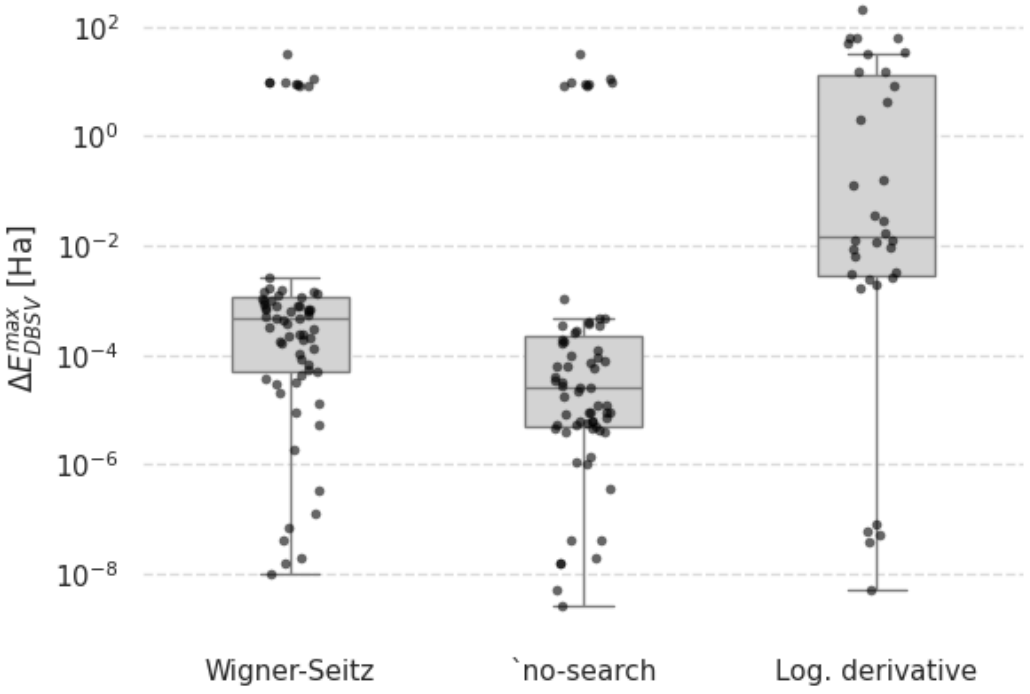


Figure (3) Boxplots of the $\Delta E^{\max}_{\mathrm{DBSV}}$ results

The DBSV results are presented in the form of the periodic table, the DBSV results indicated by a color scale. In addition, the $\ell$-channels of the valence and semicore states are indicated in the left top and bottom corners, as are the necessary SCF steps and the size of the maximized basis set in the right top and bottom corners. For better readability the tables for each method individually are included in the appendix in a larger format (Figures 8, 9, 10 and 11).

Looking at the results from the logarithmic derivative method, $\Delta E^{\max}_{\mathrm{DBSV}}$ is below $10^{-4}$ $E_{\mathrm{h}}$ only for five elements (Sc, Mn, Fe, Co, Br). For these five elements however, an exceptionally high precision at the $10^{-8}$ $E_{\mathrm{h}}$ level was reached for five elements, four of which are first row transition metals, Bromine being the exception. For these four transition metals none of the other methods could achieve a similar high precision. Moreover, these result were achieved even so the respective maximized basis sets were smaller than those from the other two methods.

For many elements the $\Delta E^{\max}_{\mathrm{DBSV}}$ result corresponding to the Wigner-Seitz method is similar to the respective result with constant linearization energies. However, the results are different by at least one order of magnitude for 26 elements, worse in 22 and better in 4 cases. Remarkably, again all the elements with significantly better results are transition metals (Mo, Re, Ru, W).

For eight elements the $\Delta E^{\max}_{\mathrm{DBSV}}$ results were particularly high (beyond 1.0 $E_{\mathrm{h}}$)

for both the Wigner-Seitz and the basis set with constant energies. These eight elements form a cluster in the main group elements of the p-block, mostly around the metalloid line. Notably, for none of these elements an $\ell = 0$ semicore state was specified, with three elements featuring no semicore state at all and five only an $\ell = 1$ semicore state. Furthermore these high $\Delta E^{\max}_{\mathrm{DBSV}}$ results coincide with relatively high values of core charge leakage (see Fig. 7 in appendix A). Taken together, this suggests a reclassification of the highest $\ell = 0$ core-state as a semi-core state in the underlying species files might lead to better results.

Overall, the sizes of the maximized basis sets are smallest for the logarithmic derivative method, on average they are 0.9 times the size of the corresponding basis sets with constant linearization energies. The Wigner-Seitz sets are almost uniformly of the same size as the 'no-search' sets. In terms of convergence speed, the maximized basis sets of the Wigner-Seitz method require an average of 15 SCF steps, just like the basis sets with constant linearization energies. The corresponding value for the logarithmic derivative method is as high as 34.

On average the linearization energies from the logarithmic derivative method are around 63 times larger than those from the 'no-search' method for the corresponding state. For the Wigner-Seitz method, this value amounts to 5.6. However, these large numbers are mostly due to the inclusion of unoccupied states, for which the 'no-search' implementation uses the relatively low value of 0.15 $E_{\mathrm{h}}$. Accordingly, when only taking occupied states into consideration the average ratio between the linearization energies deflates to 1.3 and 2.3 for the logarithmic derivative and Wigner-Seitz methods respectively. When considering only the linearization energies of semicore states, both the Wigner-Seitz and the logarithmic derivative method yield slightly lower linearization energies, than the 'no-search' method. It is further worth mentioning that the Wigner-Seitz method fails and falls back to the default value of 1.0 $E_{\mathrm{h}}$ for almost 70% of the calculated linearization energies overall. However, this mainly concerns unoccupied states, as only for 16% of the calculated valence/semicore linearization energies the default value is used. Figures 12 and 13 in Appendix A illustrate the differences in linearization energies for the example of Barium.

With all that said, it is important to recall that the DBSV test evaluates a basis sets' precision with regard to a change in the MT radius. The high precision calculations, i.e. those with small MT radius, used as a baseline in each DBSV calculation are basis set specific. Therefore, the $\Delta E^{\max}_{\mathrm{DBSV}}$ results presented above refer to a different baseline energy for each method. In order to evaluate the precision across the different methods, it is more sensible to use a common reference calculation for all methods within a given element. To this end the total groundstate energy per atom for each calculation was compared against the respective value from the high

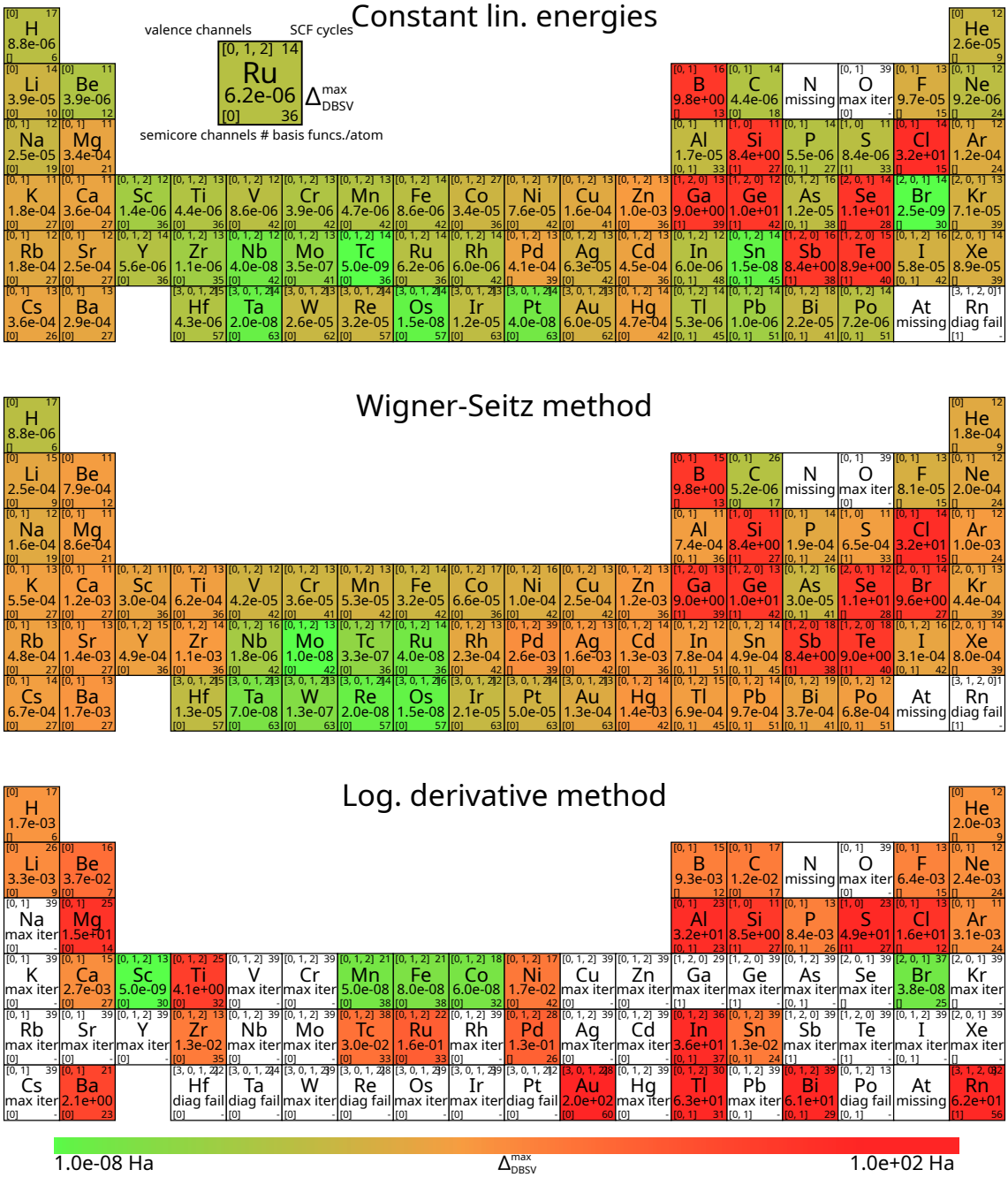


Figure (4) Results from the ‘maximize basis’ workflow runs

| | | **'no-search'** | **Wigner-Seitz** | **log. derivative** | **lcharge** |
|---|---|---|---|---|---|
| # | successful runs | 67 | 67 | 34 | 1 |
| # | best $\Delta E_{\mathrm{ns}}^{\mathrm{max}}$ results | 64 | 3 | 0 | 0 |
| | mean $\log \frac{\lvert\Delta E_{\mathrm{ns}}^{\mathrm{max}}\rvert}{E_{\mathrm{h}}}$ | 5.3e-4 | 8.2e-4 | 6.7e-1 | (9.5e-2) |
| # | $\Delta E_{\mathrm{ns}}^{\mathrm{max}} < 0\ E_{\mathrm{h}}$ | 20 | 2 | 0 | 0 |
| # | $\Delta E_{\mathrm{ns}}^{\mathrm{max}} < 10^{-2}\ E_{\mathrm{h}}$ | 59 | 59 | 8 | 0 |
| # | $\Delta E_{\mathrm{ns}}^{\mathrm{max}} < 10^{-4}\ E_{\mathrm{h}}$ | 46 | 17 | 0 | 0 |
| # | $\Delta E_{\mathrm{ns}}^{\mathrm{max}} < 10^{-6}\ E_{\mathrm{h}}$ | 25 | 2 | 0 | 0 |
| | avg. SCF iterations | 13 | 13 | 21 | (15) |
| | avg. basis size/atom | 38 | 38 | 26 | (24) |

Table (2) Summary table for $\Delta E_{\mathrm{ns}}^{\mathrm{max}}$

precision (i.e. low MT radius) reference calculation in the 'no-search' method:

$$\Delta E_{\mathrm{ns}}^{\mathrm{max}} = \frac{E^{\mathrm{max}} - E_{\mathrm{ns}}^{\mathrm{ref}}}{n} \tag{20}$$

Here $E^{\mathrm{max}}$ is the total ground state energy reached with the a given maximized basis set and $E_{\mathrm{ns}}^{\mathrm{ref}}$ is the total ground state energy from the reference calculation at low MT radius (`autormt` $= 0.75$) for the 'no-search' method. Accordingly, for the 'no-search' method $\Delta E_{\mathrm{ns}}^{\mathrm{max}} = \Delta E_{\mathrm{DBSV}}^{\mathrm{max}}$ should apply. The respective data is shown in Figure 5 and summarized in 2. Most strikingly, in 20 cases the $\Delta E_{\mathrm{ns}}^{\mathrm{max}}$ is negative (colored in blue), indicating that the respective calculation surpassed the precision of the reference value[, albeit within a $10^{-4}\ E_{\mathrm{h}}$ margin]. The is remarkable, because - as explained in Subsection 3.2 - the reference calculation is performed at a much higher plane wave cutoff than the regular calculations and highlights the importance of a proper choice of the MT radius.

Comparing the different methods in terms of $\Delta E_{\mathrm{ns}}^{\mathrm{max}}$ confirms the main result from the evaluation of the $\Delta E_{\mathrm{DBSV}}^{\mathrm{max}}$ results: the 'no-search' method is the most reliable and yields the most precise basis set for all elements, with the exception of Fluorid, where the Wigner-Seitz result is slightly lower. For those elements, where $\Delta E_{\mathrm{DBSV}}^{\mathrm{max}}$ suggested a high precision of logarithmic derivative base sets however, the $\Delta E_{\mathrm{ns}}^{\mathrm{max}}$ data disproves these assumptions. The high accuracies in terms of $\Delta E_{\mathrm{DBSV}}^{\mathrm{max}}$ are merely a consequence of the poor results in the respective DBSV benchmark calculations. Accordingly, the logarithmic derivative base sets produce $\Delta E_{\mathrm{ns}}^{\mathrm{max}}$ results that are $6.7 \cdot 10^{-1} E_{\mathrm{h}}$ higher on average than the high precision 'no-search' benchmark, while the 'no-search' methods results are within a $5.3 \cdot 10^{-4}\ E_{\mathrm{h}}$ margin of this reference on average. The respective average for the Wigner-Seitz basis sets lies in between these two values ($8.2 \cdot 10^{-4}\ E_{\mathrm{h}}$). In summary, the maximized basis sets with constant linearization energies are most robust with respect to variation in the MT radius,

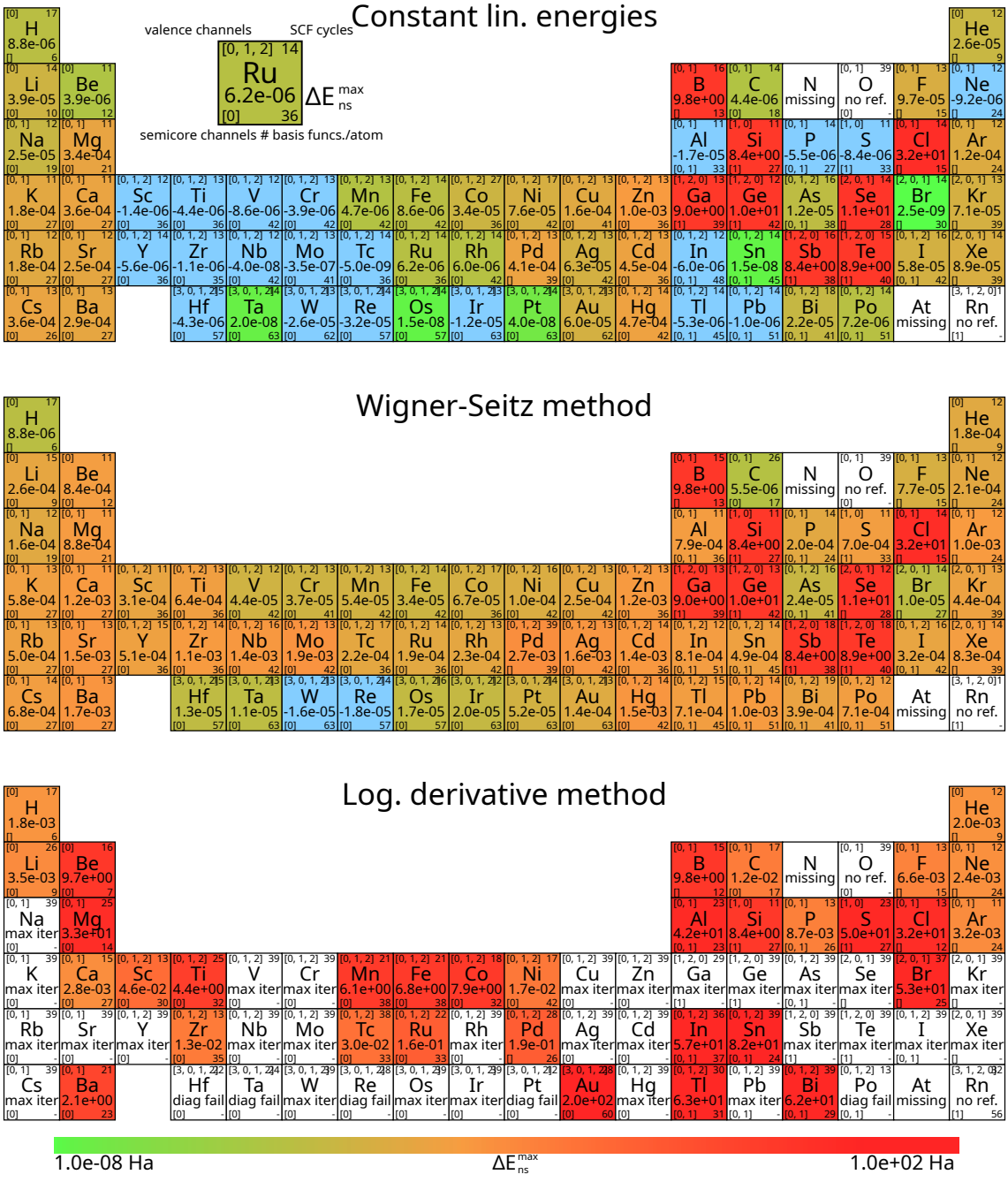


Figure (5) Differences in total ground state energy per atom regarding the DBSV reference calculation with low MT radius of the 'no-search' method.

as shown by the results of the $\Delta E^{\max}_{\mathrm{DBSV}}$ tests. They are also the most accurate with respect to the achievable ground state energies, as shown by the $\Delta E^{\max}_{\mathrm{ns}}$ results. The next chapter presents the results of the LO hierarchies, which compare the basis functions in terms of their efficiency.

## 4.2 Local orbital hierarchies

As explained, in Subsection 3.2, the workflow orders the LOs within a maximized basis sets with regard to their importance to the total ground state energy. This allows to examine the minimal necessary basis set size in order to achieve a given accuracy threshold. Again, in order to be able to compare the results across the different methods, the energies from the low MT radius calculation for the maximized 'no-search' basis set $E^{\mathrm{ref}}_{\mathrm{ns}}$ served as a reference:

$$\Delta E_{\mathrm{ns}} = \frac{E - E^{\mathrm{ref}}_{\mathrm{ns}}}{n} \tag{21}$$

$n$ is the number of atoms in the unit cell and $E$ is the achieved total ground state energy achieved with a given basis set. Figure 6 lists the minimal necessary basis set size per atom to achieve a $10^{-4}$ $E_{\mathrm{h}}$ accuracy with regard to $\Delta E_{\mathrm{ns}}$. Figures 14 and 15 in Appendix A show the respective results for the $10^{-6}$ $E_{\mathrm{h}}$ and $10^{-8}$ $E_{\mathrm{h}}$ accuracies. Unfortunately, there was an error when setting the parameters for the LO hierarchy workflow. The result was that the workflow did use the correct `exciting` species files from each method, indicating which types of LOs and APW to include for each state, but it did not apply the respective method in the calculations determining the hierarchy. Instead it fell back to the usage of the 'no-search method' for all its calculations. Accordingly, the results are exactly the same for the Wigner-Seitz and 'no-search' methods, as their respective maximized basis sets always included the same combination of LOs. For all elements and accuracy levels, the same minimum basis size is required between the two. Only the logarithmic derivative methods shows worse results for some elements, due to the smaller maximized basis sets used as the input of the LO hierarchy workflow. Unfortunately, the error was not noticed in time for the corrected results to be reported. Reruns of the LO hierarchy workflow with corrected settings are ongoing at the time of the submission of this thesis.

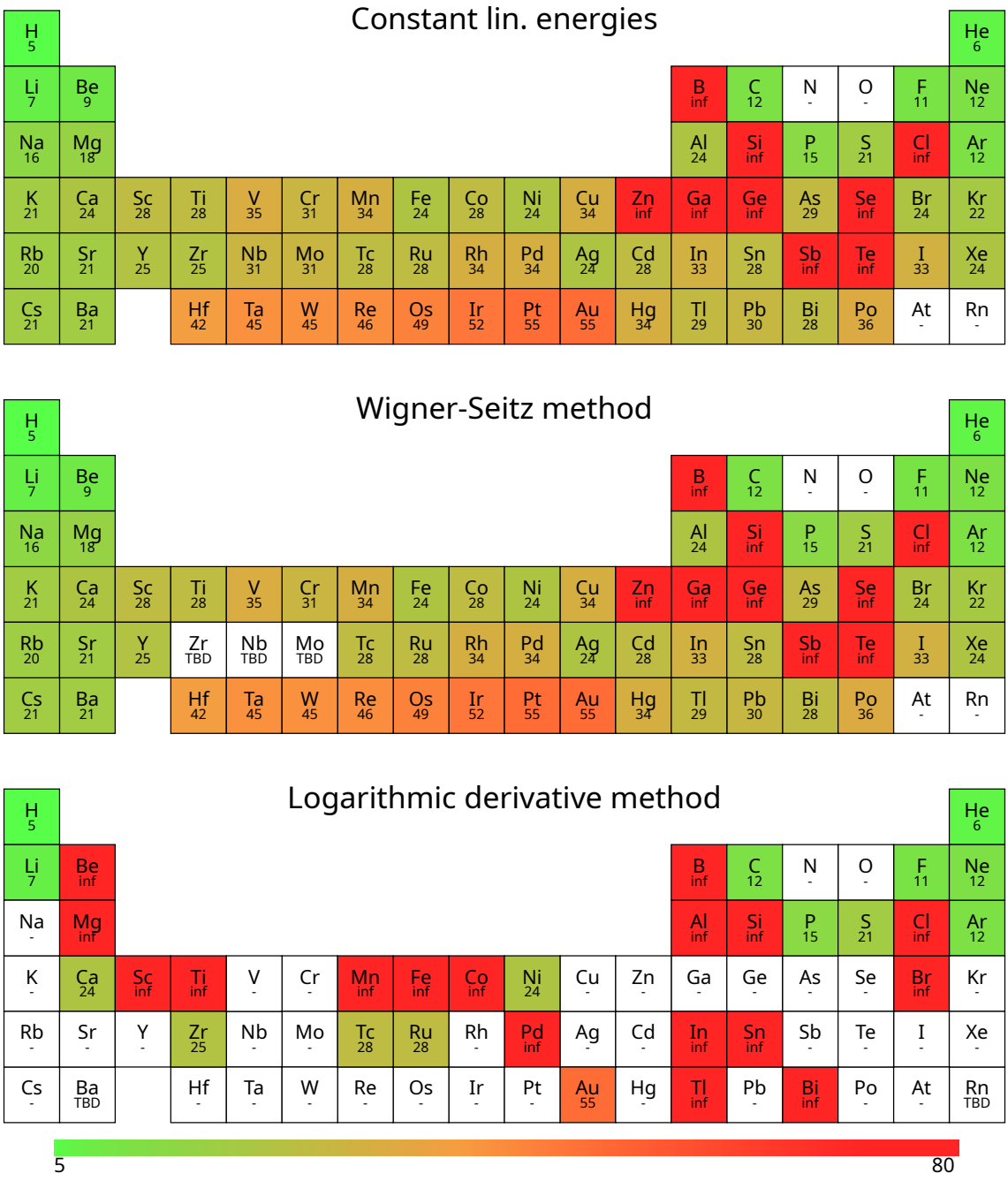


Figure (6) Minimal required basis set size per atom for $\Delta E_{\mathrm{ns}} < 10^{-4}\ E_{\mathrm{h}}$ accuracy

# 5 Conclusion

The '$\ell$-like charge' method has proven unsuitable to determine linearization energies in the present study. On a methodological level, the method is irreconcilable with the local orbitals $\varphi^{\alpha}_{\ell m}$ (see Eq. 19) used to describe the semicore states, as they include two distinct linearization energies for the respective $\ell$-channel. The '$\ell$-like charge' method only provides one such value by averaging across the different bands in the respective channel. On the implementation level, the many errors within the first SCF iteration (see Fig. 11), indicate that the initialization of uniform starting values $E_\ell = 0.15\ E_\mathrm{h}$ for all $\ell$-channels may be a problem as well. The logarithmic derivative method too has proven to be unreliable for building maximized basis sets. The workflow provided a valid result in only half of all tested cases, when using this method. None of these were able to provide a total ground state energy within a $10^{-3}\ E_\mathrm{h}$ margin of the benchmark for the respective element. The result is somewhat surprising as logarithmic derivative method proved successful in previous studies. However, both Betzinger et al. [11] and Michalicek et al. [10] used the it only with regards to the linearization energies for certain (high energy) local orbitals. In contrast, in this thesis a given method was always applied to the entire basis set, in particular also to the APW functions. The application of the Wigner-Seitz method resulted in maximized basis sets that provide total ground state energies within a $10^{-3}\ E_\mathrm{h}$ margin of the respective benchmark values on average. The method frequently failed to determine the appropriate energy window and used the hard-coded $1.0\ E_\mathrm{h}$ fall-back value. It be useful to change this value to $0.15\ E_\mathrm{h}$, which has proven a useful default value in many species files. For all but one of the tested elemental crystals (Fluorine) using constant linearization energies provided the most accurate maximized basis sets. The respective 'no-search' method results are within $10^{-4}\ E_\mathrm{h}$ margin of the benchmark on average. Unfortunately, the results from the LO hierarchy workflow are void with regard to comparing the different methods, due to an improperly set parameter. The reruns are currently ongoing and yet to be evaluated.

It is worth noting, that the four tested methods vary in two different respects: (1) the criterion according to which the specific values of the linearization energies are calculated (Eqs. 1, 2, 3) and (2) whether these values are continuously updated during the course of an SCF cycle or not. Regarding the first aspect, the Wigner-Seitz rules (Eq. 12) seem to provide the most precise and robust results. Regarding the second aspect, the superior results of the 'no-search' method over the Wigner-Seitz method suggest, that leaving the linearization energies constant within the SCF cycle is the better approach. It might be worth testing if this conclusion holds true for the logarithmic derivative criterion (16) as well. However, the current implementation in `exciting` does not readily provide this functionality. The use of constant linearization energies currently also implies the use of the Wigner-Seitz

rules in first iteration, i.e. the the 'no-search' method.

The DBSV test methodology resulted in some misleading results regarding the quality of the basis sets, especially for the logarithmic derivative method. This suggests that the choice of the linearization energies has considerable influence on the behavior of the resulting radial functions not only towards the MT boundary - as previously assumed - but also further inside of the MT sphere. A further decrease in the `autormt` parameter for the DBSV test calculation might improve the tests validity.

For future research it might worth testing, if the results from the Wigner-Seitz or logarithmic derivative method can be approved upon, when limiting their use to only certain types of basis functions. i.e. distinguishing between semicore and valence states or LOs and APW functions.

# References


[1] Andris Gulans et al. “Exciting: a full-potential all-electron package implementing density-functional theory and many-body perturbation theory”. In: *Journal of Physics: Condensed Matter* 26.36 (2014), p. 363202.

[2] Pierre Hohenberg and Walter Kohn. “Inhomogeneous electron gas”. In: *Physical review* 136.3B (1964), B864.

[3] Walter Kohn and Lu Jeu Sham. “Self-consistent equations including exchange and correlation effects”. In: *Physical review* 140.4A (1965), A1133.

[4] David S Sholl and Janice A Steckel. *Density functional theory: a practical introduction*. Second. John Wiley & Sons, 2023.

[5] David J Singh and Lars Nordstrom. *Planewaves, Pseudopotentials, and the Lapw Method*. en. 2nd ed. New York, NY: Springer, Dec. 2006.

[6] John C Slater. “Wave functions in a periodic potential”. In: *Physical Review* 51.10 (1937), p. 846.

[7] D D Koelling and G O Arbman. “Use of energy derivative of the radial solution in an augmented plane wave method: application to copper”. In: *Journal of Physics F: Metal Physics* 5.11 (Nov. 1975), p. 2041. URL: https://doi.org/10.1088/0305-4608/5/11/016.

[8] O Krogh Andersen. “Linear methods in band theory”. In: *Physical Review B* 12.8 (1975), p. 3060.

[9] David Singh. “Ground-state properties of lanthanum: Treatment of extended-core states”. In: *Phys. Rev. B* 43 (8 Mar. 1991), pp. 6388–6392. URL: https://link.aps.org/doi/10.1103/PhysRevB.43.6388.

[10] Gregor Michalicek et al. “Elimination of the linearization error and improved basis-set convergence within the FLAPW method”. In: *Computer Physics Communications* 184.12 (2013), pp. 2670–2679.

[11] Markus Betzinger et al. “Local exact exchange potentials within the all-electron FLAPW method and a comparison with pseudopotential results”. In: *Physical Review B—Condensed Matter and Materials Physics* 83.4 (2011), p. 045105.

[12] Martí Raya-Moreno et al. *An exciting approach to theoretical spectroscopy*. 2026. URL: https://arxiv.org/abs/2601.11388.

[13] OK Andersen. “Simple approach to the band-structure problem”. In: *Solid State Communications* 13.2 (1973), pp. 133–136.

[14] L Hodges, RE Watson, and H Ehrenreich. “Renormalized atoms and the band theory of transition metals”. In: *Physical Review B* 5.10 (1972), p. 3953.

[15] Peter Blaha et al. *wien2k. An augmented plane wave+ local orbitals program for calculating crystal properties*. Vol. 60. 1. Vienna University of technology Austria, 2001, pp. 155–169.

[16] Ferenc Karsai, Fabien Tran, and Peter Blaha. "On the importance of local orbitals using second energy derivatives for d and f electrons". In: *Computer Physics Communications* 220 (2017), pp. 230–238.

[17] Stefan Blügel and Gustav Bihlmayer. "Full-potential linearized augmented planewave method". In: *Computational nanoscience: do it yourself* 31 (2006), pp. 85–129.

[18] Alexander Buccheri et al. "Excitingtools: An exciting workflow tool". In: *Journal of Open Source Software* 8.85 (2023), p. 5148.

[19] Kurt Lejaeghere et al. "Reproducibility in density functional theory calculations of solids". In: *Science* 351.6280 (2016), aad3000.

[20] Claudia Draxl and Matthias Scheffler. "The NOMAD laboratory: from data sharing to artificial intelligence". In: *Journal of Physics: Materials* 2.3 (May 2019), p. 036001. URL: https://doi.org/10.1088/2515-7639/ab13bb.

# A Appendix

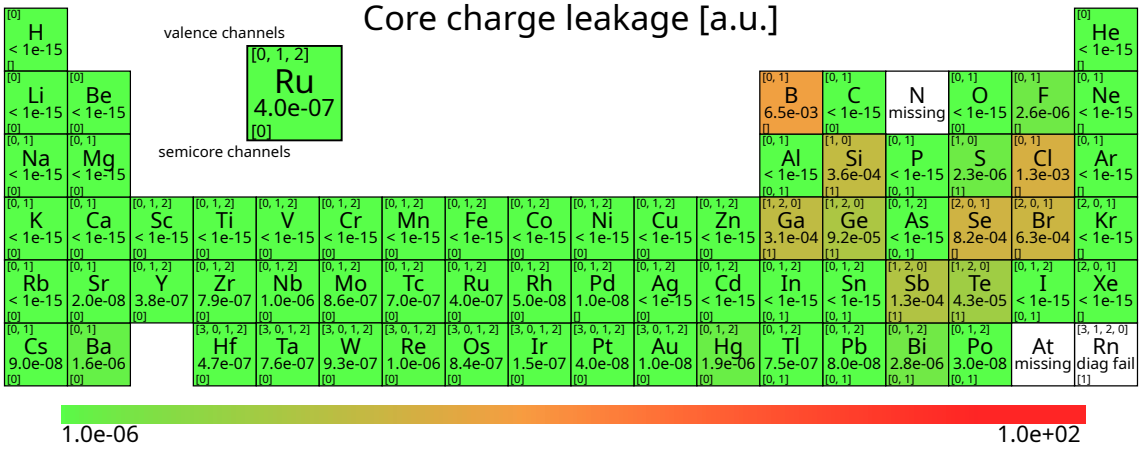


Figure (7) Core leakage from maximized basis sets with constant linearization energies (`autormt` = 0.95)

| **Abbreviation** | **`exciting` error codes** |
|---|---|
| deg. rad | degenerate local-orbital radial functions<br>degenerate APW radial functions<br>gs_degen_apw_rad |
| diag fail | diagonalization failed<br>gs_diag_fail |
| no info.out | gs_info_out_file_missing |
| max iter | gs_max_iter |
| no Fermi | could not find Fermi energy |
| timeout | time_out |
| missing | not included in test set |
| other | gs_generic_error |

Table (3) Error code abbreviations

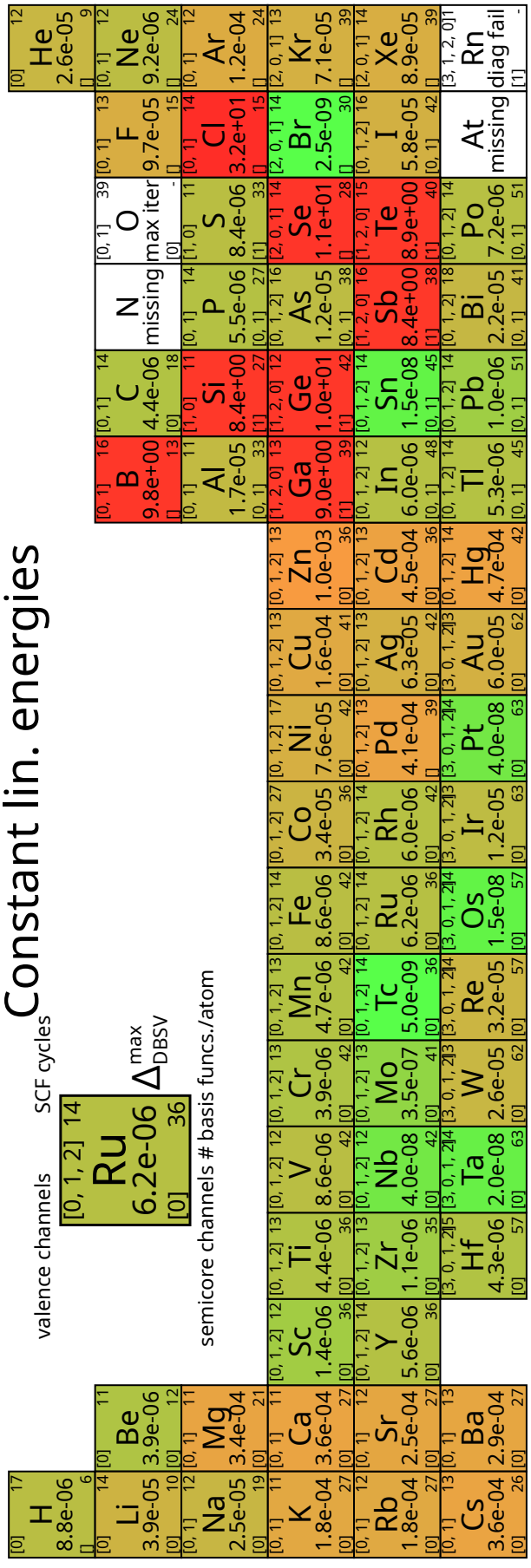


Figure (8) Results from the 'maximize basis' workflow runs for the 'no-search' method

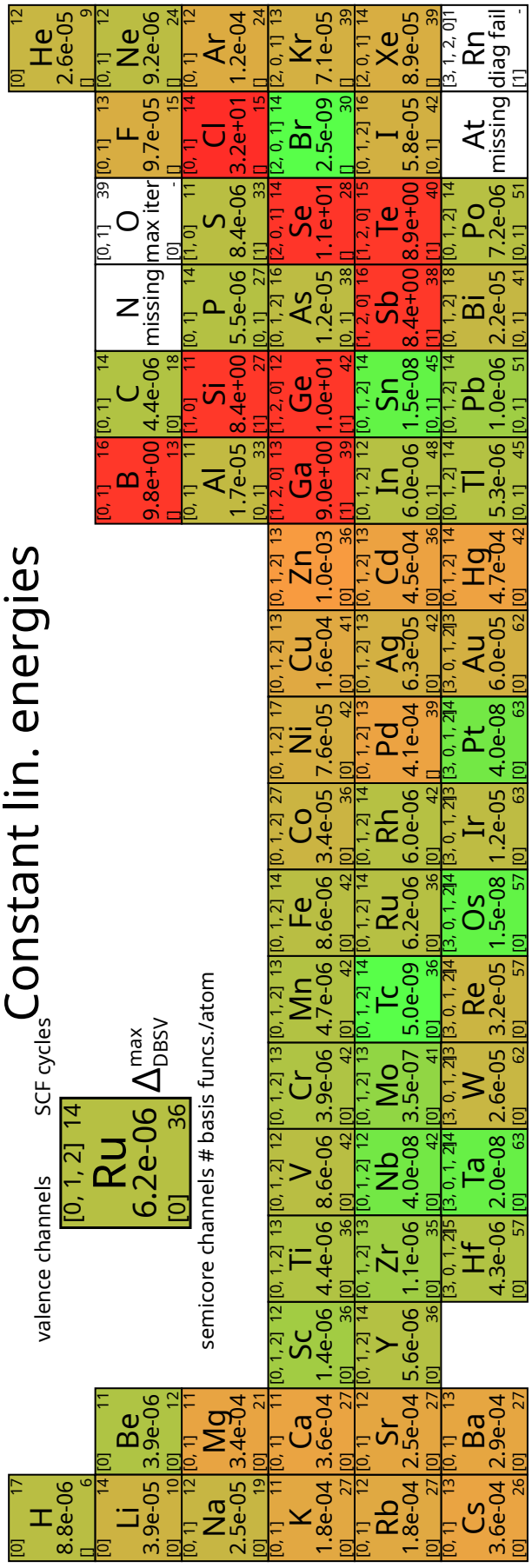


Figure (9) Results from the 'maximize basis' workflow runs for the Wigner-Seitz method

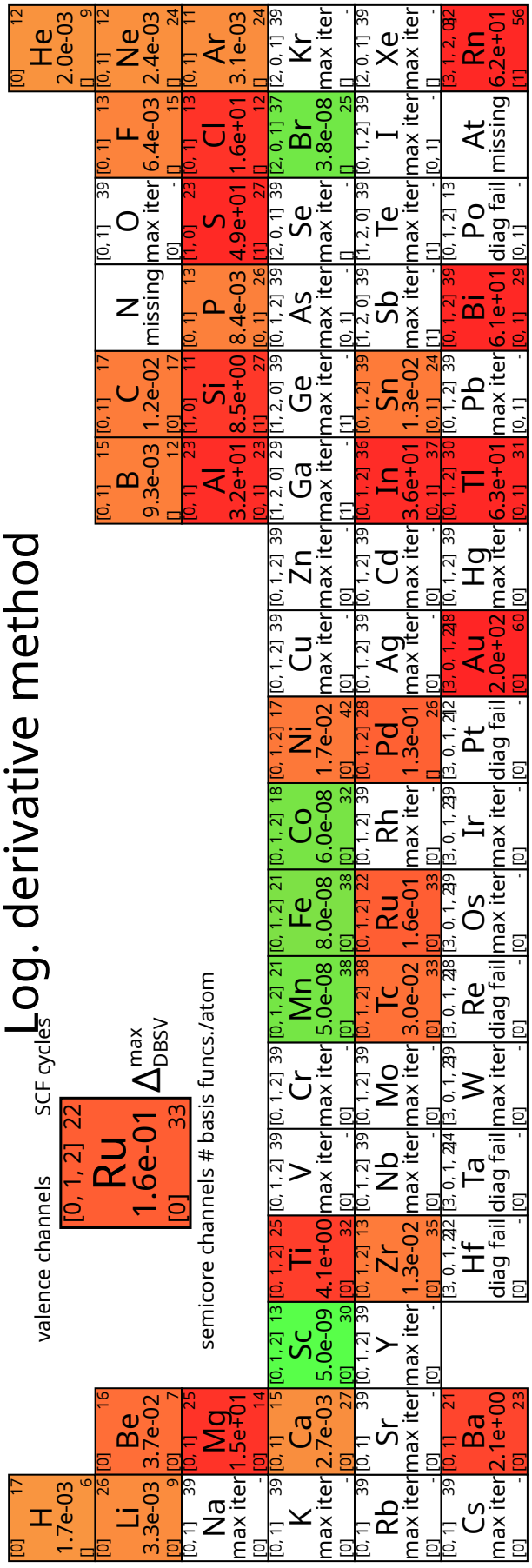


Figure (10) Results from the 'maximize basis' workflow runs for the logarithmic derivative method

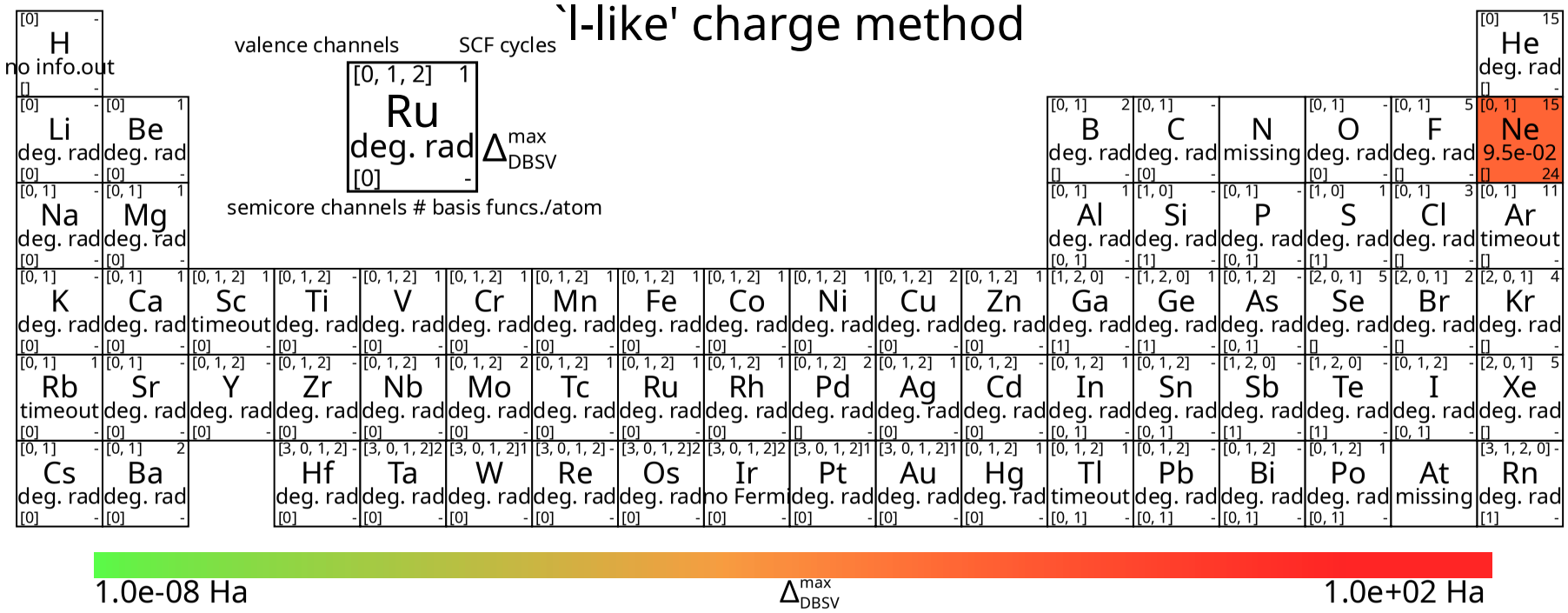


Figure (11) Results from the 'maximize basis' workflow runs for the '$\ell$-like charge' method

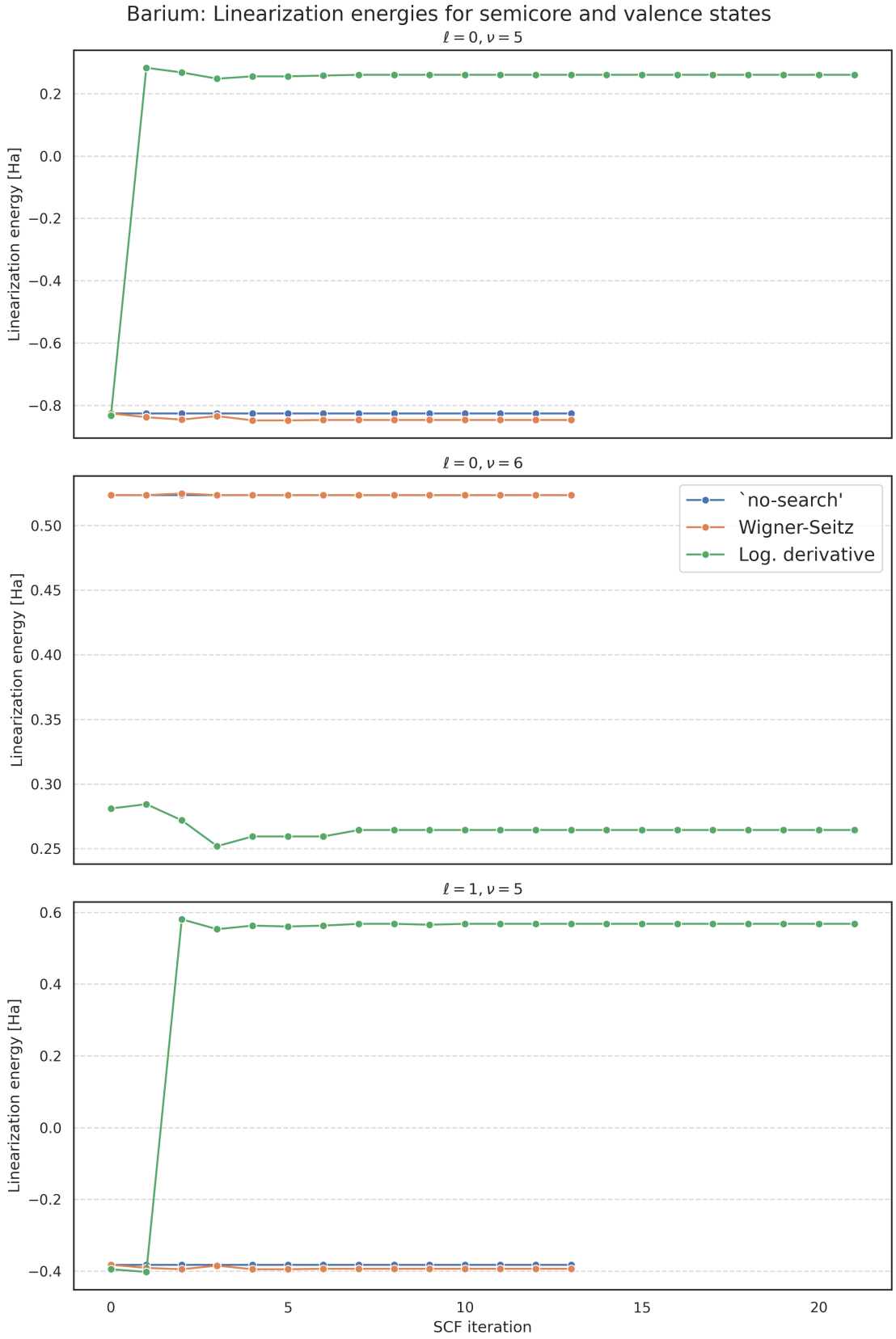


Figure (12) Linearization energies from Barium semicore and valence states for the different methods

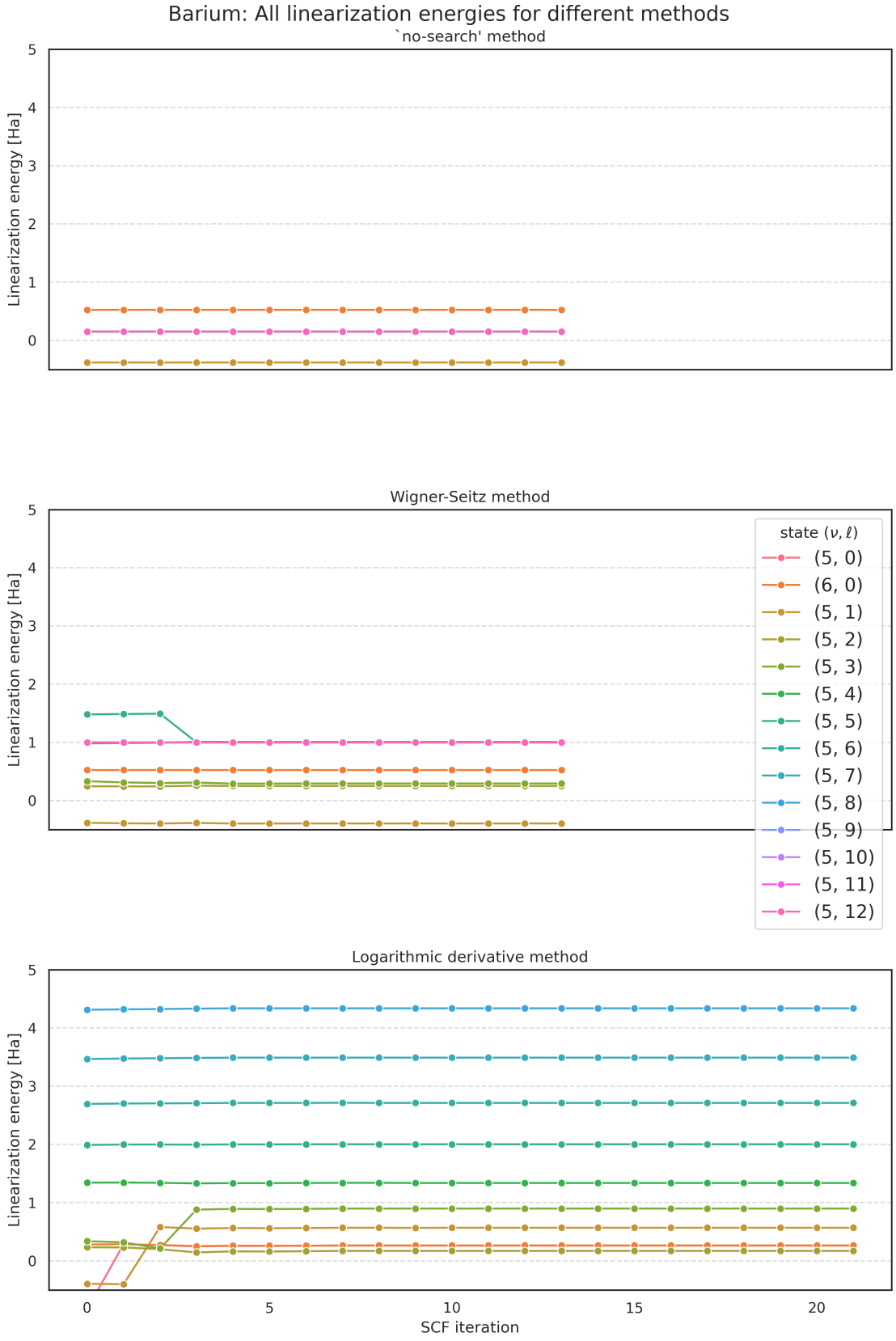


Figure (13) Linearization energies from all non-core states in Barium

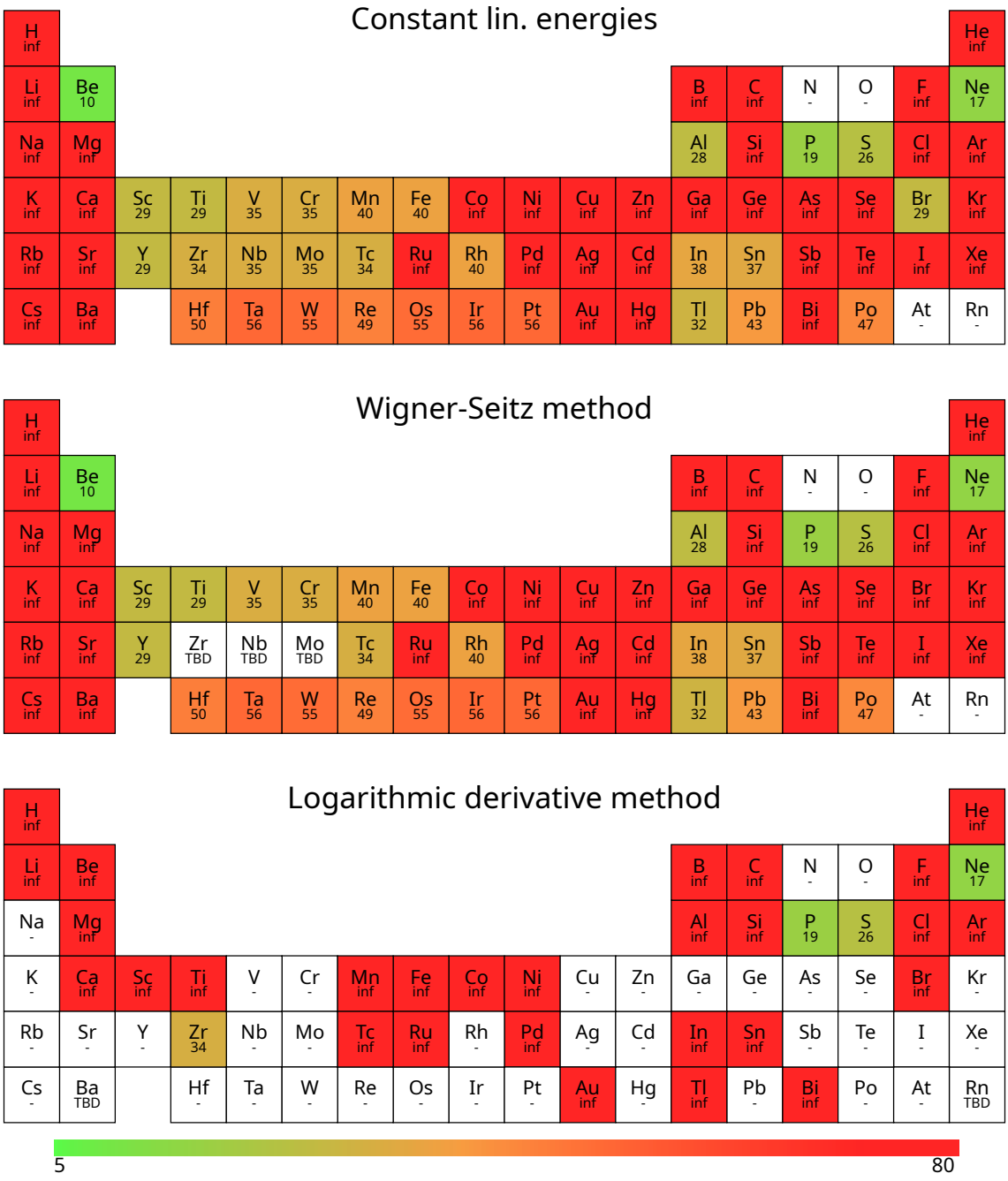


Figure (14) Minimal required basis set size per atom for $\Delta E_{\mathrm{ns}} < 10^{-6}\ E_{\mathrm{h}}$ accuracy

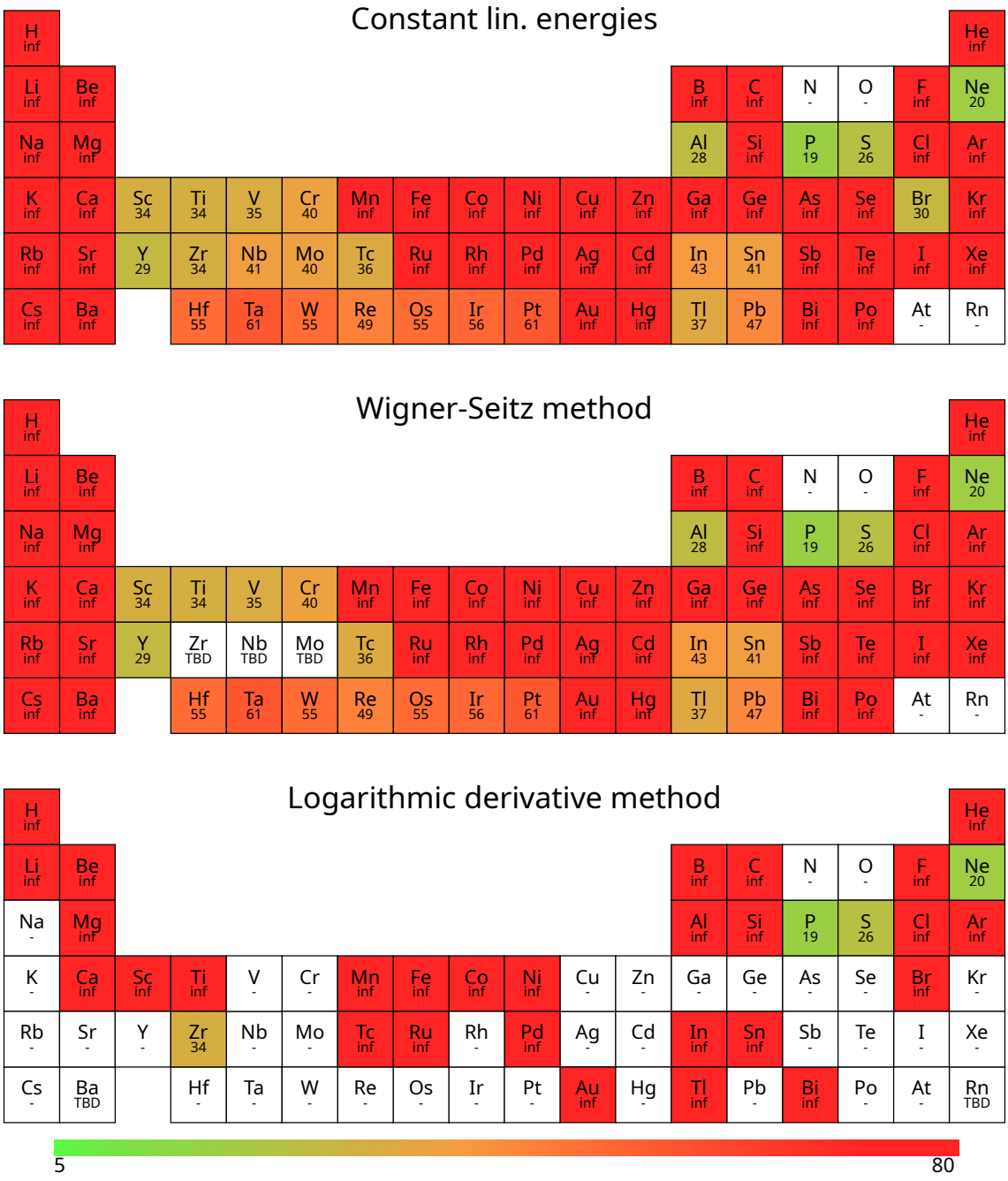


Figure (15) Minimal required basis set size per atom for $\Delta E_{\mathrm{ns}} < 10^{-8}\ E_{\mathrm{h}}$ accuracy

# B Declaration of originality

**Selbstständigkeitserklärung**

Ich erkläre hiermit, dass ich die vorliegende Arbeit selbstständig verfasst und noch nicht für andere Prüfungen eingereicht habe. Sämtliche Quellen einschließlich Internetquellen, die unverändert oder abgewandelt wiedergegeben werden, insbesondere Quellen für Texte, Grafiken, Tabellen, Bilder sowie die Nutzung von Künstlicher Intelligenz für die Erstellung von Texten und Abbildungen, sind als solche kenntlich gemacht. Mir ist bekannt, dass bei Verstößen gegen diese Grundsätze ein Verfahren wegen Täuschungsversuchs bzw. Täuschung eingeleitet wird.

Berlin: February 23, 2026